INVESTIGATING THE BACTERIAL ADHESION BEHAVIOUR ON BONE SURFACE MIMICKED CHITOSAN MEMBRANES

by

Meltem Uçak

B.S., in Bioengineering, Yildiz Technical University, 2016

Submitted to the Institute of Biomedical Engineering
in partial fulfillment o f t he requirements
for the degree of
Master of Science
in
Biomedical Engineering

Boğaziçi University
2022

ACKNOWLEDGMENTS

First, I want to express my gratitude to Prof. Dr. Bora Garipcan for his guidance throughout my master's degree. Dr. Garipcan, thank you for admitting me into this program and for your support of my experiments. Without his valuable contribution to choosing my PhD scholarship location, I would not decide where I should lead to.

I want to express my gratitude to you, my family, for having supported and believed in me all my academic life without losing their belief in me. They have been my hope to get this degree whenever I feel tired.

My dear lab members, I am very thankful for what I learned from you. It was a pleasure to meet all of you and work together without individual agenda. I wish you luck and best in the academic circle for long years.

It is essential to credit some special friends for their mental support during this thesis, dear Ayhan. I am fortunate to have a friend like you.

Finally, I want to thank myself for everything. Meltem, whenever you reminisce on this period of your life, remember that you accomplished this. Allow this thesis to remind you of all the time and effort you put into this program. Although I encountered various problems in this effort, with the help of my family and friends, I dealt with those.

ACADEMIC ETHICS AND INTEGRITY STATEMENT

I, Meltem UÇAK, hereby certify that I am aware of the Academic Ethics and Integrity Policy issued by the Council of Higher Education (YÖK) and I fully acknowledge all the consequences due to its violation by plagiarism or any other way.

Name :

Signature:

Date:

ABSTRACT

INVESTIGATING THE BACTERIAL ADHESION BEHAVIOUR ON BONE SURFACE MIMICKED CHITOSAN MEMBRANES

An extremely serious post-op consequence of orthopedic replacement surgery is infection, which is currently challenging to treat with antibiotics. According to data, prosthesis infections correlate with biofilm formation that is highly resilient to host immune defenses and antibiotics. The main goal of this thesis is to examine the relationship between topography and surface-cell and surface-bacteria interactions. The secondary objective is to determine whether it is possible to chemically alter potential implant surfaces and their topographical features to maximize cell-implant interactions while minimizing bacterial-implant interactions. Physicochemical characterization for Graphene Oxide (GO) coated bone surface mimicked Chitosan (BSM-CH-GOc) loaded Ampicillin sodium salt (Amp) or Tetracycline hydrochloride (Tetra) membranes were done via degradation test, Scanning Electron Microscopy (SEM) and drug release study. For cell study, mouse fibroblast (L929) was selected as a model mammalian cell line. Bacterial behavior on these membranes was investigated using the biofilm growth test. The rate of biofilm production was assessed and utilized as an indication in which *Escherichia Coli* (ATCC 8739) and *Staphylococcus aureus* (ATCC 6538) were utilized as model organisms. It was found that while GO coated bone surface mimicked chitosan membranes had a noticeable effect on preventing bacterial biofilm formation, the presence of ampicillin sodium salt and tetracycline hydrochloride remarkably reduced the biofilm formation compared to the control groups.

Keywords: Surface-cell interactions, Surface-bacteria interactions, Chitosan, Ampicillin, Tetracycline.

ÖZET

KEMİK YÜZEYİ TAKLİT EDİLEN KİTOSAN MEMBRANLARINDA BAKTERİYEL TUTUNMA DAVRANIŞLARININ İNCELENMESİ

Proteze bağlı enfeksiyon, hali hazırda antibiyotik ile tedavisi zor olan ortopedik eklem yenileme cerrahisinin ciddi bir ameliyat sonrası komplikasyonudur. Kanıtlar, protez enfeksiyonlarının, antibiyotik tedavisine ve konakçı bağışıklık tepkilerine oldukça dirençli, biyofilm ile ilişkili enfeksiyonlar olduğunu göstermektedir. Bu çalışmanın temel amacı, topografya ile yüzey-hücre ve yüzey-bakteri etkileşimleri arasındaki ilişkiyi ve her birinin önemini incelemektir. İkincil bir amaç, bakteri-implant etkileşimlerini en aza indirirken hücre-implant etkileşimlerini en üst düzeye çıkarmak için topografik özelliklerini değiştirerek implant yüzeylerini kimyasal olarak değiştirmenin mümkün olup olmadığını belirlemektir. Ampisilin veya tetrasiklin içeren BSM-CH-GOc membranlar için fizikokimyasal karakterizasyon, bozunma testi, ilaç salım çalışması ve Taramalı Elektron Mikroskobu (SEM) yoluyla yapılmıştır. Hücre çalışması için fare fibroblastı (L929) model memeli hücre hattı olarak seçilmiştir. Bu membranlar üzerindeki bakteriyel davranış, bakteriyel biyofilm oluşturma testi (MTT testi) kullanılarak araştırılmıştır. Gram pozitif ve gram negatif bakteriler *Staphylococcus aureus* ve *Escherichia Coli* model organizma olarak kullanılarak biofilm oluşma hızı ölçülmüş ve bir gösterge olarak kullanılmıştır. Kemik yüzey taklidi grafen oksit kaplı kitosan membranların bakteri biyofilm oluşumunu önlemede gözle görülür bir etkiye sahipken, ampisilin sodyum tuzu ve tetrasiklin hidroklorür varlığının kontrol gruplarına kıyasla biyofilm oluşumunu önemli ölçüde azalttığı bulunmuştur.

Anahtar Sözcükler: Yüzey-hücre etkileşimleri, Yüzey-bakteri etkileşimleri, Kitosan, Ampisilin, Tetrasiklin.

TABLE OF CONTENTS

LIST OF FIGURES

LIST OF TABLES

LIST OF ABBREVIATIONS

Amp	Ampicillin Sodium Salt
BSM	Bone Surface Mimicked
BSM-CH	Bone surface mimicked Chitosan
BSM-CH-GOc	Graphene Oxide coated bone surface mimicked Chitosan
CH	Chitosan
DMEM	Dulbecco's modification of Eagle medium
DMSO	Dimethyl sulfoxide
E. coli	*Escherichia Coli*
FBS	Fetal Bovine Serum
GO	Graphene Oxide
LB	Lysogency broth
MTT	3-(4,5- dimethylthiazol-2-yl)-2,5-diphenyltetrazolium bromide
Plain-CH	Plain Chitosan
Plain-GOc	GO coated plain chitosan
PBS	Phosphate-Buffered Saline
PBMS	Poly(dimethylsiloxane)
S.aureus	*Staphyloccus Aureus*
Tetra	Tetracycline Hydrochloride
TSB	Tryptic Soy Broth
UV	Ultraviolet

1. INTRODUCTION

1.1 Motivation

Orthopedic joint replacement surgeries are performed considerably more frequently each year. According to the 2021 American Joint Replacement Registry Annual Report, 2,244,587 primary and revision knee and hip arthroplasty surgeries were carried out between 2012 and 2020. The primary knee (54.5%) and primary hip (38.6%) operations were the most prevalent. Arthroplasty failure is caused by aseptic or mechanical loosening, dislocations, prosthesis infections, fractures, osteolysis, or wound complications. Infection was the primary cause of hip revision surgery, contributing 20.1 percent of all cases. An early revision occurs within three months of the first procedure. Infection (32.9%) was the primary reason for all early hip revisions. Moreover, infection and inflammatory reaction placed top in the All-Knee Revisions list (25.2%), and inflammatory reaction and infection (63.9%) were again the principal factors for early knee surgery [1].

Orthopedic joint replacement surgery has a major post-operative complication called a prosthesis-related infection, which is currently difficult to treat with antibiotics. The most used method to treat the infection is usually to remove the infected prosthesis. To prevent infections of prosthetic devices, it is crucial to comprehend the complex relationship between infectious microorganisms and host immune responses. Finding demonstrates prosthesis infections correlate with biofilm formation that is highly resilient to host immune defenses and antibiotics [2].

Biofilm formation by colonized bacteria chronically infects surrounding tissues and can also increase antibiotic resistance by up to 10,000-fold [3]. Due to the restricted ability to treat the infection noninvasively, typical clinical practice is to completely remove the device before administering stronger systemic antibiotics. However, the period is greatly extended by device-associated infections, and the following revision

procedures needed to treat them it takes for patients to recover, increase the expense of healthcare, and increase the risk of bacterial recolonization [4].

Chitosan is a prevalent and frequently utilized natural polymer which originates from chitin deacetylation, when under acidic conditions, is found to be the only occurring naturally cationic polysaccharide since the acidic conditions protonate the lateral amino group [5]. Such characteristics and properties include stimulus responsiveness, biodegradability, impermeability to oxygen, antibacterial properties, and biocompatibility [6]. Due to these properties, CH is widely used in the drug delivery, healing wounds and regenerative medicine [7, 8, 9]. Moreover, chitosan is a polysaccharide, making it susceptible to a diverse variety of chemical modifications due to having reactive functional groups. Chitosan polymers benefit from these reactive groups since they can be treated readily to generate membranes, scaffolds, and nanofiber and to modify with micro and nanoparticles [10]. Such nanoparticles can include carbon-based, polymeric, and inorganic nanoparticles [11], [12]. The combination of graphene oxide (GO) has garnered the most interest of all of them.

CH and GO can be successfully combined to design biomaterials with exceptional biocompatible capacity, mechanical performance. As a result, a substantial corpus of research has been done on the use of membranes constructed of GO and CH in a variety of sectors, with biomaterials being the most prevalent [13]. Due to their vast surface area and richness of amino and oxygen-containing functional groups, Graphene oxide coated chitosan materials are ideal candidates for biopolymer and drug delivery. The constructed delivery systems have a substantial loading capacity for drugs and an extended-release rate, so graphene oxide coated chitosan materials can be targeted using magnetic nanoparticles or ligands [14]. Additionally, CH-GO 3D materials are capable of supplying a setting that promotes proliferation, cell migration and differentiation. All of them exhibit strong osteo-inductive activity. CH-GO based biomaterial are, therefore, essential for tissue engineering, especially bone regeneration [15]. Additionally, due to CH-GO systems' outstanding antibacterial activity against variety of bacteria, it is thought that they play a key role in wound dressings [16], [17].

The focus of current research in this field, however, has been chiefly on maximizing the capabilities of the two bioactive components themselves, ignoring the requirement for creating distinctive micro- and nano-topographies. Surface topography can significantly alter the bone formation rate or an antibacterial agent's effectiveness [18].

Ampicillin sodium salt (Amp) is a well-known, effective broad-spectrum antibiotic used for many years to treat bacterial infections via prevents bacteria from synthesizing cell walls [19]. For instance, ampicillin-loaded polymeric fibers have been used locally to treat infections in various situations, including wound healing [20].

Tetracycline hydrochloride (Tetra) is an antibiotic group derived from the genus Streptomyces. By preventing these microorganisms from synthesizing proteins, it is effective against a variety of gram positive and gram-negative bacteria [21]. In a recent study illustrates that tetracycline loaded chitosan nanoparticles improved the antibacterial properties of fabrics [22].

Overall, more emphasis should be placed on developing CH-GO based biomaterials with topographic characteristics. Additionally promising is the simultaneous integration of several distinct properties, including anti-bacterial, hemostasis, and tissue regeneration.

1.2 Aim

The primary aim of this thesis is to examine the correlation between topography on both surface-cell and surface-bacteria interactions as well as their importance. The secondary aim is investigating the possibility of chemically modifying implant surfaces and changing topography properties to optimize cell implant interactions but also to minimize bacteria-implant interactions.

As a result, the findings of this thesis will contribute to closing a significant gap

in our knowledge of the relationship between bacterial behavior and surface characteristics of biomaterials that mimic bone surface.

In this way we will be able to reveal dynamics of that relation and utilize the knowledge in designing biomaterials. Our main goal is to investigate how bone surface mimicked Chitosan-Graphene Oxide Coated membranes affect bacterial adhesion behavior.

The objectives to achieve and main goals of the study are following;

1. To mimic topography of the bone surface onto PDMS (Poly dimethyl siloxane) membranes via soft lithography technique.
2. To fabricate bone surface mimicked (BSM) Chitosan-Graphene oxide (CH-GO) coated membranes.
3. To load ampicillin sodium salt and tetracycline hydrochloride to CH-GO membranes.
4. Investigate the structure, morphology, bactericidal effect, and anti-biofilm activity of BSM-CH-GOc loaded ampicillin sodium salt and tetracycline hydrochloride membranes against the strain of *E. coli* and *S. aureus*.
5. Study of the cytotoxicity of ampicillin sodium salt and tetracycline hydrochloride on mammalian cell viability.

2. BACKGROUND

2.1 Formation of Bacterial Biofilms

Bacteria can easily colonize on the synthetic material and device surfaces, like those implanted within the human body. When bacteria attach to the surface, they begin to divide and form colonies. As the colony grows, biofilm, also known as "extracellular polymeric substances" or "EPS", or bacterial encapsulation within a protective polysaccharide coating that keeps the bacteria together via sugary molecular strands, develops. The cells' EPS production makes the development of intricate, three-dimensional, robust, attached communities. Depending on the environment, biofilms can be several inches thick or as thin as a few cell layers. Additionally, biofilm can use biological signaling molecules to 'communicate' between cells to coordinate action. Since the creation of biofilms shields dangerous bacteria from drugs and are one of the main factors in the development of chronic infections, biofilms are recognized as a significant concern [23, 24, 25].

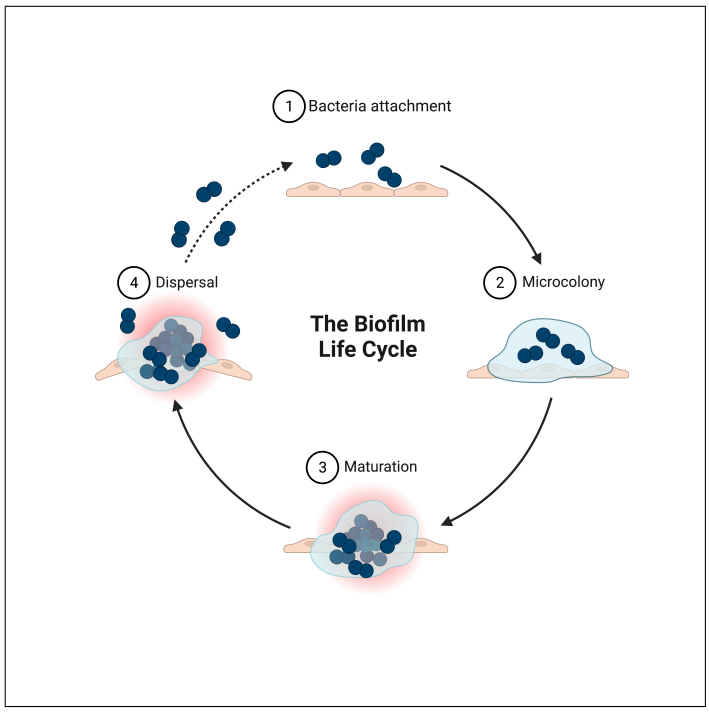

Figure 2.1 The biofilm life cycle (Created using Biorender.com).

2.2 Function of Bacterial Cell Wall

The functionality of the bacterial cell wall is to give it rigidity, strength, and shape while also shielding it from mechanical and osmotic damage [26]. Bacterial cell walls can be split into two groups: Gram positive (+) and Gram negative (-), each of which has a distinct structure, composition, and function. Teichoic acids, which are specific to the Gram-positive cell wall, make up the cell wall of Gram-positive bacteria and a thick coating of peptidoglycan (PG) that is 20-50 nm thick. Gram-negative cell walls, on the other hand, have more intricate chemical and structural compositions. More precisely, the outer membrane that encloses the surface membrane and a thin PG layer make up the Gram-negative bacteria's cell wall. Lipopolysaccharides, a unique component of the outer membrane of Gram-negative bacteria enhance the negative charge of cell membranes by frequently providing resistance to hydrophobic chemicals and being essential for the structural integrity and survivability of the bacteria [27].

When it comes to bacterial resistance to antibiotics or susceptibility to them, as well as the diffusion of antibiotics into biofilm matrixes, the composition, and characteristics of the cell wall of bacteria might be critical [28], [29].

2.3 CH-GO Based Material

CH and GO are easily able to construct different systems through covalent bonding, hydrogen bonding, or electrostatic interactions because of the several functional groups that can interact with one another. Recent studies have demonstrated that there is a synergistic effect that occurs between CH and GO. This synergy creates a hybrid system which ameliorated optical qualities and thermal stability [30],[31]. In addition, the synergistic effect is displayed in, *in vivo* and *in vitro* biocompatibility [32], angiogenic, the effect of cell growth [33], and also antimicrobial properties [34].

2.3.1 Bone Tissue Engineering

CH-based composites and systems contain many advantageous characteristics such as the stimulating regeneration, repairing damaged tissue, reducing costs, and accelerating recovery [35]. CH-GO nanocomposites are promising systems; given the constant improvement of GO, they could contribute to the advancement of tissue engineering [36]. The examination of CH-GO nanocomposites in bone tissue engineering is of utmost importance; the rationale for this is that CH's molecular structure is similar to that of glycosaminoglycan [37]. Furthermore, GO and CH combination exhibits the ability to promote osteogenic differentiation [38].

2.3.2 Drug Delivery

GO is widely used in drug and biomacromolecule delivery since GO nanocarriers can carry many drugs. This is primarily due to GO's large surface area, π-conjugated structure, and surface activity which is derived from oxygen-containing functional groups [39]. Additionally, CH, when encountered with the acidic solid tumor media, it becomes positively charged which aids in cellular uptake given the attraction of positively charged nanocarriers to negatively charged tumor cell membranes [40].

3. MATERIALS AND METHODS

3.1 Preperation of Bone Template

The femur bone was obtained from a local butcher and pretreated prior to use. The xenograft cleaning procedure was used. Bovine femurs were chopped into pieces with a bone saw and then placed in absolute ethanol for 30 minutes before being transferred into a 10% NaCl solution for 24 hours. To remove lipids and other potential residues from the surface of the bone chips were submerged in acetone for 20 minutes after that for 72 hours, 2 hours, and 144 hours in 3% H_2O_2, 2M NaOH, and acetone, respectively, to eliminate inactive prions and immunologic structures. Chips of cleansed bone were chemically dried overnight [41].

3.2 Bone Surface Mimicked (BSM) Mold Preparation

To replicate the negative surface topography of the femur bone's surface, soft lithography was employed with PDMS (Sylgard 18, Dow Corning, Midland, MI) and a silicone elastomer to curing agent ratio of 10:1. After being prepared and expelled of gas, the PDMS solution was applied to the surface of the previously treated bone. This was followed by a 4-hour incubation period at 65 $^{\circ}C$. Lastly, PDMS polymer layer was peeled off and detached from the bone surface. PDMS was copied bone surface structures on its surface, and bone surface mimicked mold made of PDMS was utilized [41].

3.3 Fabrication of Bone Surface Mimicked Chitosan based Membranes

Low molecular weight chitosan (50,000-190,000 Da) and Graphene Oxide were bought from Sigma Aldrich. 2.5 g of pure chitosan was dissolved in a 2.5% aqueous acetic acid solution to prepare the chitosan solution and stirring it overnight. Then, CH-based membranes were fabricated using the solvent casting method [42]. The solution was poured onto the bone negative mold and smooth PDMS substrate to construct the bone surface mimicked and plain membranes. To remove any air bubbles, the samples were degassed for one hour and were left to dry at 65 $°C$ overnight in an oven. Once the membranes were dried, they were collected and immersed in a 1 M NaOH solution for one hour. They were then rinsed with DI water before being stored at 4 $°C$ [43]. The surface of the BSM-CH membranes was coated with GO using a 0.5 mg/mL GO solution that was produced and exfoliated using an ultrasonic homogenizer for 1 hour at 50 kHZ in an ice bath. The exfoliated Graphene Oxide solution was then poured over the dry membranes and kept there overnight at 4$°C$ after receiving a 2-minute UV-Ozone treatment. The samples were cleaned twice with distilled water and then put back into storage at 4 $°C$ to be used at a later [44].

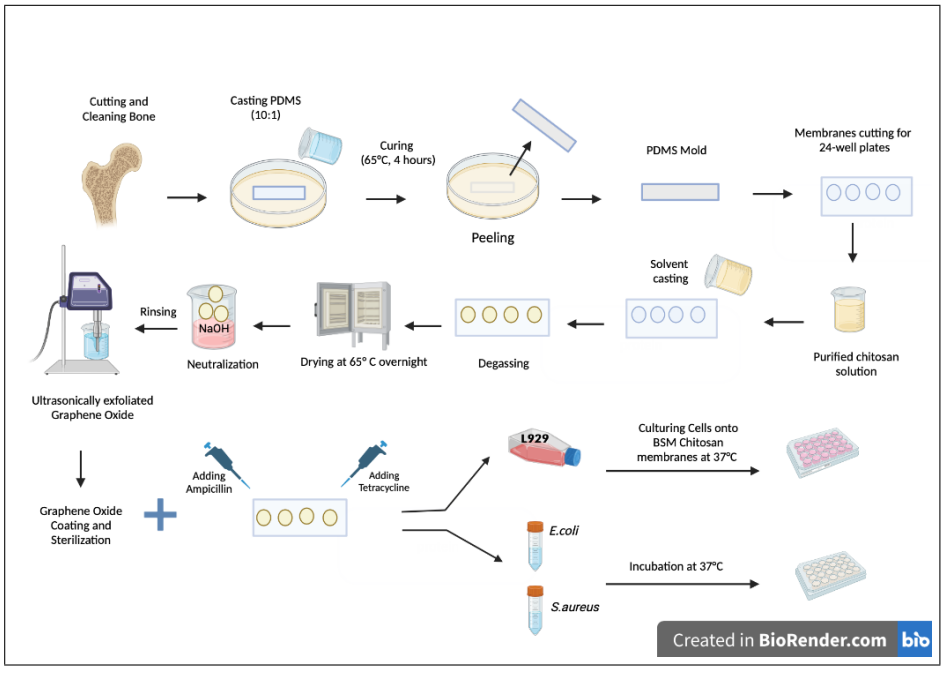

Figure 3.1 Schematic depiction of the overall experimental procedures.

3.4 Characterization of Materials

3.4.1 Scanning Electron Microscopy (SEM)

The samples were coated with 5 nm-thick layers of gold to be examined under a microscope. Using a Scanning Electron Microscope (SEM), the bone surface images were taken to make sure the surface topography of the bone was accurately mimicked along with a PDMS mold and the mimicked CH membranes of the bone surface. The images of SEM were captured utilizing Philips XL30 ESEMFEG/EDAX equipmentat 5.00 kV and 15 mm working distance.

3.4.2 Water Contact Angle (WCA) Measurements

Utilizing a contact angle measuring device, the water contact angles of chitosan membranes were measured. Deionized water droplets in the amount of 10μL were dropped onto several experimental groups, and circle fitting was used to measure the water contact angles. Water contact angels for Plain-CH, Plain-CH-GOc, BSM-CH, BSM-CH-GOc, Ampicillin sodium salt loaded BSM-CH-GOc membranes (A1, A3, A5, A10) and Tetracycline hydrochloride loaded BSM-CH-GOc membranes (T0.5, T1, T3, T5) were measured.

3.4.3 Degradation Test

Tetra and Amp stock solutions were prepared using deionized water. $300\,\mu$L of antibiotics solution was added to each BSM-GOc membranes, with final concentrations of $1\,\mathrm{mgmL^{-1}}$, $3\,\mathrm{mgmL^{-1}}$, $5\,\mathrm{mgmL^{-1}}$, $10\,\mathrm{mgmL^{-1}}$ for Amp loaded groups arranged as A1, A3, A5, A10. In the same way, with the final concentrations of $0.5\,\mathrm{mgmL^{-1}}$, $1\,\mathrm{mgmL^{-1}}$, $3\,\mathrm{mgmL^{-1}}$, $5\,\mathrm{mgmL^{-1}}$ for Tetra- loaded groups arranged as T0.5, T1, T3, T5.

Initially, materials were dehydrated at 65 °C for 48 hours before adding the enzyme solution. After each membrane's dry weight was determined. 750 μL of freshly produced 0.8 mg mL^{-1} lysozyme enzyme in dH_2O was added to the wells of 24-well plates comprising dehydrated membranes. Plates were then incubated for an additional 21 days at 37 °C. Every three days, the solution was changed. On days 7, 14, and 21, the dry weights of all samples were evaluated, and the degradation incidences were computed using Eq. 3.1:

$$Weight\,Loss\,Ratio = \frac{(W_0 - W_t)}{W_0} \tag{3.1}$$

W_t represents sample weight on day t and W_0 represents the initial dehydrated sample weight.

3.4.4 Drug Release Studies

Firstly, the dried membranes were weighed and immersed in 1mL of PBS (Phosphate Buffered Saline) at 37°C. After the measurement was made at the end of 24 hours, the PBS was refreshed, and the measurement was made after waiting for another 24 hours. The amount of released Tetra and Amp into PBS was quantified by using a UV-VIS spectrophotometer (NanoDrop^{TM} 2000 Spectrophotometer, Thermo Scientific^{TM}) at 220 nm and 340 nm [45].

3.5 L929 Cell Culture Studies

Cell viability was used to measure the interactions between mammalian cell lines and plain and BSM membranes to further understand the impact of chemistry and surface topography. Therefore, the mouse fibroblast (L929) cell line was selected

as a model mammalian cell line. The L929 cells were seeded with a density of 3.5×10^4 cells per well on 24-well cell culture-treated plates making use of DMEM (Dulbecco's modification of Eagle medium).

A 10% Fetal Bovine Serum (FBS) was used along with a 1% v/v antibiotic (penicillin-streptomycin) were used to supplement the growth mediums. Additionally, viability test was carried out on the first, second, and third days. An MTT solution (3-(4,5- dimethylthiazol-2-yl)-2,5-diphenyltetrazolium bromide) was prepared with a concentration of 5mg/mL using a filtered PBS (pH=7.2) and added at a ratio of 1:10 was incubated at 37 °C for 3.5 hours. This solution was used to quantify viability. After the incubation period, the medium was disposed, and adding Dimethyl sulfoxide (DMSO) caused the formazan crystals to dissolve. With the aid of a microplate reader (iMark Microplate Absorbance Reader, BioRAD Laboratories, US), optical density was measured at 570 nm and 750 nm wavelengths.

3.6 Bacteria Studies

3.6.1 Biofilm Growth Test

Staphylococcus Aureus (ATCC 6538) and *Escherichia Coli* (ATCC 8739) were used as model organisms in this measurement of biofilm formation rate on the chitosan based membranes. Each bacterial strain 100 μL was suspended and grown overnight and were added to 10 mL LB and TSB medium. They were then supplemented using 100μL of 50% w/v glucose solution to help with biofilm growth. The bone surfaced mimicked membranes and sterilized plain membranes were put into a 24-well plate along with 750 μL of bacterial suspension onto each sample. The plates were then placed into a stationary incubator for 24 hours at 37 °C. Following that, the samples were taken out of the well plates and gently dipped into PBS individually in order to remove the detached bacteria. Comparative analysis was done between the biofilm that formed on the membranes and the tissue culture plate used as the control group. This was done through the evaluation of the viability by means of percentages of metabolic

activity by performing a MTT assay [46].

3.6.2 Analysis of Zone of Inhibition on Drug-Loaded BSM-CH-GOc Membranes

The zone of inhibition test was carried out to determine the susceptibility to two antibiotics of the bacteria using Ampicillin sodium salt loaded BSM-CH-GOc membranes and Tetracycline hydrochloride loaded BSM-CH-GOc membranes. This test show how sensitive or resistant bacteria of interest is to various antibiotics. Firstly, 5 mm diameter circles of samples were prepared. Both Ampicillin sodium salt doses at different concentrations (A1, A3, A5, A10) and Tetracycline hydrochloride (T0.5, T1, T3, T5) were loaded onto the BSM-CH-GOc membranes.To produce the plates, tryptic soy agar (TSA) was used. On the agar plates, 10^7 CFU of the model bacteria *Staphylococcus aureus* (ATCC 6538) in 100 mL of Lysogency broth (LB) and *Escherichia Coli* (ATCC 8739) in 100 μL of TSB (Tryptic Soy Broth) were dispersed using an L-spreader. The samples were then put on the agar plates. The diameter of each inhibitory zone was determined by a caliper in mm (n=6) following a 24-hour incubation period at 37 °C [47].

4. RESULTS

4.1 Scanning Electron Microscopy (SEM)

SEM was used to obtain images of the femur bone, PDMS mold, and the bone surface mimicked the chitosan membrane to ensure that the surface topography of bone was accurately mimicked. The images are represented in Figure 4.1.

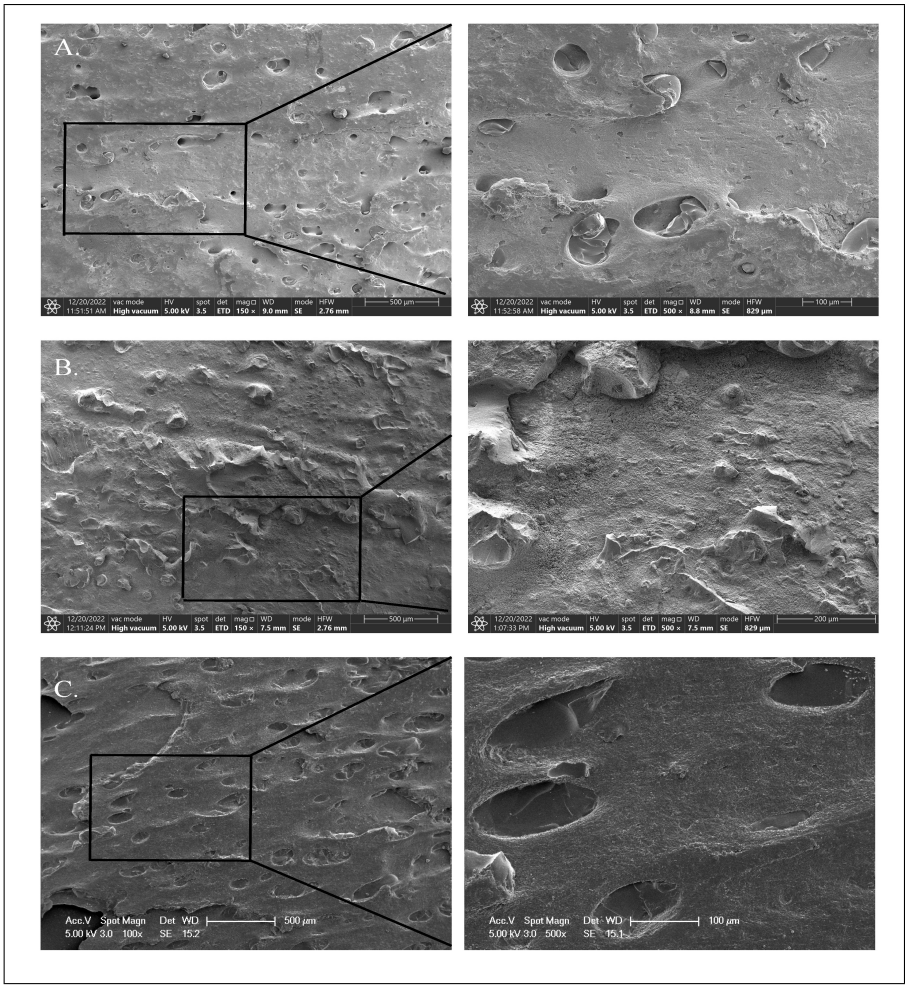

Figure 4.1 Comparing the surface topographies of the femur bone, PDMS mold, and bone surface mimicked chitosan membrane. (A) SEM images of bovine femur bone surface topography. (B) SEM images of the PDMS mold surface topography. (C) SEM images of the BSM-CH membrane.

4.2 Water Contact Angle Measurements

Water contact angles were measured to assess the hydrophobicity and hydrophilicity of chitosan-based membranes. Water contact angels for Plain-CH, Plain-CH-GOc, BSM-CH, BSM-CH-GOc, Ampicillin sodium salt loaded BSM-CH-GOc membranes (A1, A3, A5, A10) and Tetracycline hydrochloride loaded BSM-CH-GOc membranes (T0.5, T1, T3, T5) were measured and results were given in Table 4.1. The result indicates that compared to BSM-CH-GOc, Amp loading increases the water contact angle in A1, while the amount of antibiotic decreases in WCA, and A10 has the lowest WCA among all groups, which is $39.29\,^{\circ} \pm 2.75$.

Contrary to the Amp-loaded groups, the water contact angle increases as antibiotics increase in the Tetra-loaded groups. In addition, it was seen that coating the surface with GO increased WCA in the Plain-CH group, while it decreased it in the BSM-CH groups. Ampicillin-loaded membranes exhibit more hydrophilicity, whereas Tetra membranes exhibit greater hydrophobicity.

Table 4.1
Water Contact Angle Values of Chitosan Membranes.

Experimental Groups	Average (°)	St. Dev
A1	66.49	1.81
A3	42.61	1.26
A5	55.77	0.43
A10	39.29	2.75
T0.5	74.17	1.16
T1	79.18	0.31
T3	67.95	3.04
T5	83.82	0.65
Plain-CH	60.86	1.05
Plain-CH-GOc	75.26	1.46
BSM-CH	66.50	0.95
BSM-CH-GOc	59.11	5.39

4.3 Degradation Test

Enzymatic degradation of Plain-CH, Plain-CH-GOc, BSM-CH, BSM-CH-GOc, Ampillin loaded BSM-CH-GOc membranes, and Tetra loaded BSM-CH-GOc membranes were conducted using lysozyme enzyme. Figure 4.2A and 4.2B illustrates the degradation rate of drug-loaded BSM-CH-GOc membranes decreases considerably as the antibiotics concentration increases. Also, surface coating with GO has a similar effect on degradation, as seen in Figure 4.2C. According to the data, the average degradation % of Tetra-loaded and Amp-loaded BSM-CH-GOc membranes after 21 days was 5.1% and 4.9%, respectively. BSM-CH membrane has the highest degradation rate, followed by T0.5, A1, and Plain-CH, according to measurements.

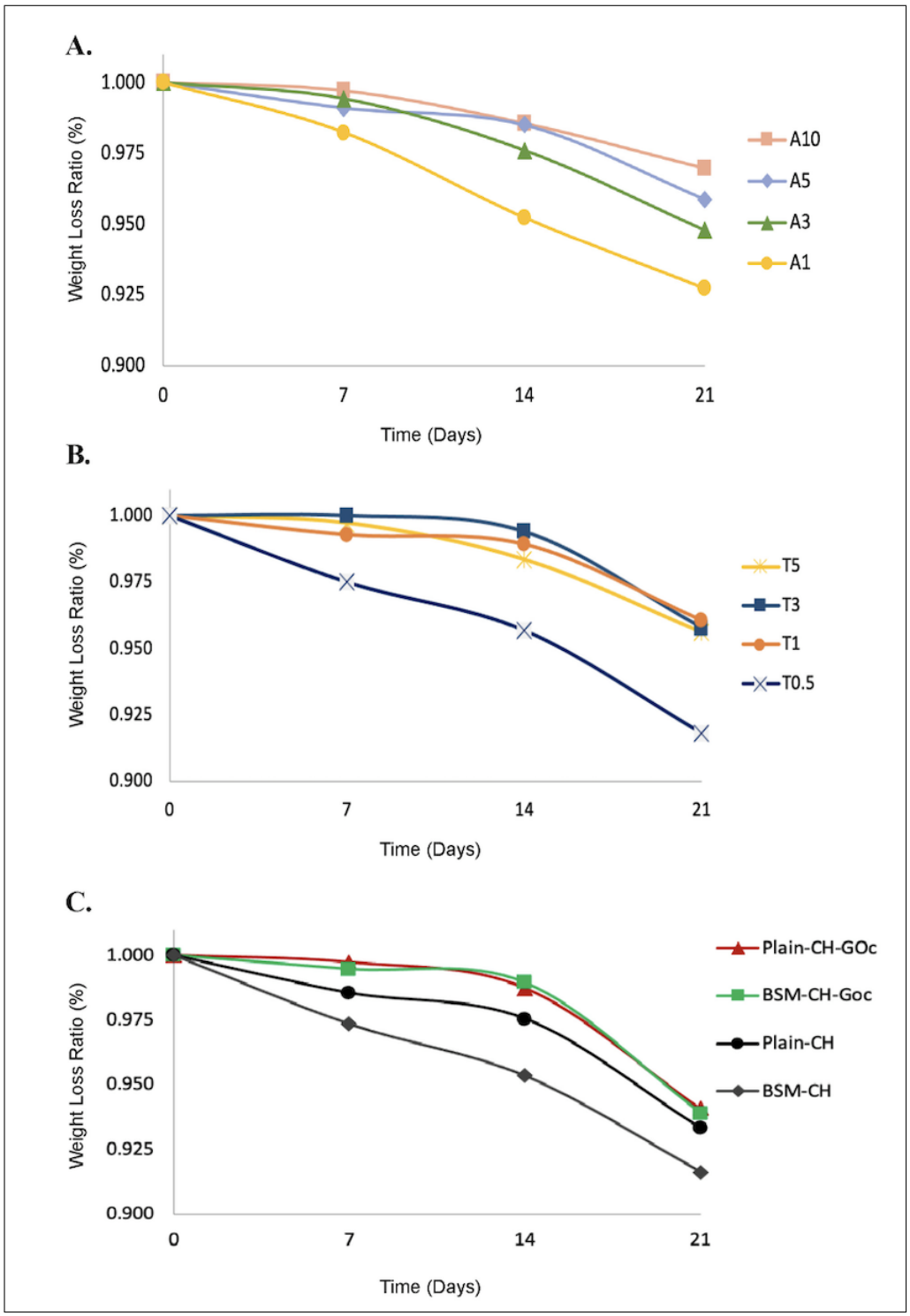

Figure 4.2 Degradation rate of chitosan-based membranes in phosphate buffer saline solution. (A) Amp loaded BSM-CH-GOc membranes. (B) Tetra loaded BSM-CH-GOc membranes. (C) Plain-CH: Plain Chitosan, BSM-CH: Bone surface mimicked chitosan, Plain-CH-GOc: Graphene Oxide coated plain chitosan, BSM-CH-GOc: Graphene Oxide coated bone surface mimicked chitosan.

4.4 Drug Release Profile

During 48-hour incubation in PBS at 37 °C, the drug release study was conducted to determine the release profile of Amp and Tetra from BSM-CH-GOc membranes. The reason why the release at 24 and 48 hours is highlighted on the Figure 4.3 is to see how much the release was on the 1^{st} and 2^{nd} days when biofilm formation was measured. The overall analysis of this data revealed that while Tetra loaded groups remained stable after 24 hours, the release was observed in Amp loaded groups.

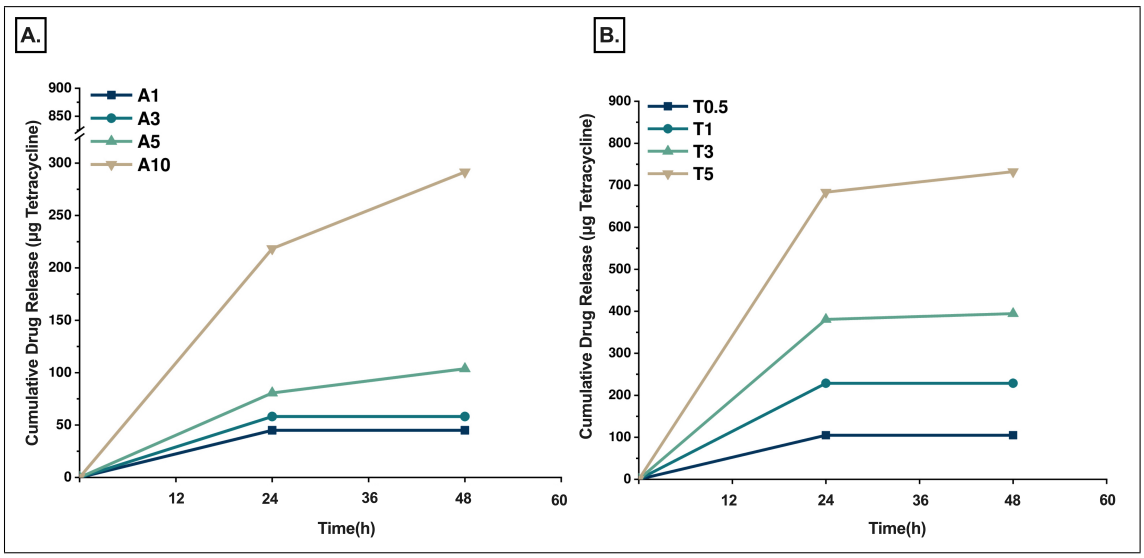

Figure 4.3 Results of drug release. (A) Release of Amp-groups during 48 h incubation in PBS at 37 °C. (B) Release of Tetra loaded groups during 48h incubation in PBS at 37 °C (Amp: ampicillin sodium salt, A1: 1 $mgmL^{-1}$ Amp, A3: 3 $mgmL^{-1}$ Amp, A5: 5 $mgmL^{-1}$ Amp, A10: 10 $mgmL^{-1}$ Amp, Tetra: Tetracycline hydrochloride, T0.5: 0.5 $mgmL^{-1}$ Tetra, T1: 1 $mgmL^{-1}$ Tetra, T3: 3 $mgmL^{-1}$ Tetra, T5: 5 $mgmL^{-1}$ Tetra).

4.5 Cell Culture Studies

L929 MTT assay was conducted to assess any possible cytotoxicity that may have been caused by the presence of two different antibiotics: ampicillin sodium salt and tetracycline hydrochloride inside graphene oxide-coated bone surface mimicked chitosan membranes on cell viability.

Plain-CH, Plain-CH-GOc, BSM-CH, and BSM-CH-GOc were compared with the MTT assay to find out the best group. A considerable disparity between the groups was found to exist. [$F(5, 10) = 3.537, p = 0.0479$, two-way ANOVA; Figure 4.4].

Tukey's multiple comparisons were carried out to understand the source of this difference among groups. Post hoc comparisons using Tukey's test indicated that there is a significant difference between the Plain-CH and Plain-CH-GOc for the cell viability on day 3 ($M_{\text{Plain-CH}} = 55.66$, $M_{\text{Plain-CH-GOc}} = 76.94$, SE of diff $= 2.705, p < 0.001$). There is also a paramount difference between Plain-CH and BSM-CH for the cell viability on day 3 ($M_{\text{Plain-CH}} = 55.66$, $M_{BSM-CH} = 86.86$, SE of diff $= 3.309, p < 0.001$). Lastly, a significant difference between Plain-CH and BSM-CH-GOc for the cell viability both on day 1 and day 3 was found as well ($M_{\text{Plain-CH}} = 55.66$, $M_{BSM-CH-GOc} = 85.31$, SE of diff $= 4.275, p < 0.001$). After the L929 cell viability results, the BSM-CH-GOc group was chosen as the best group to continue the thesis.

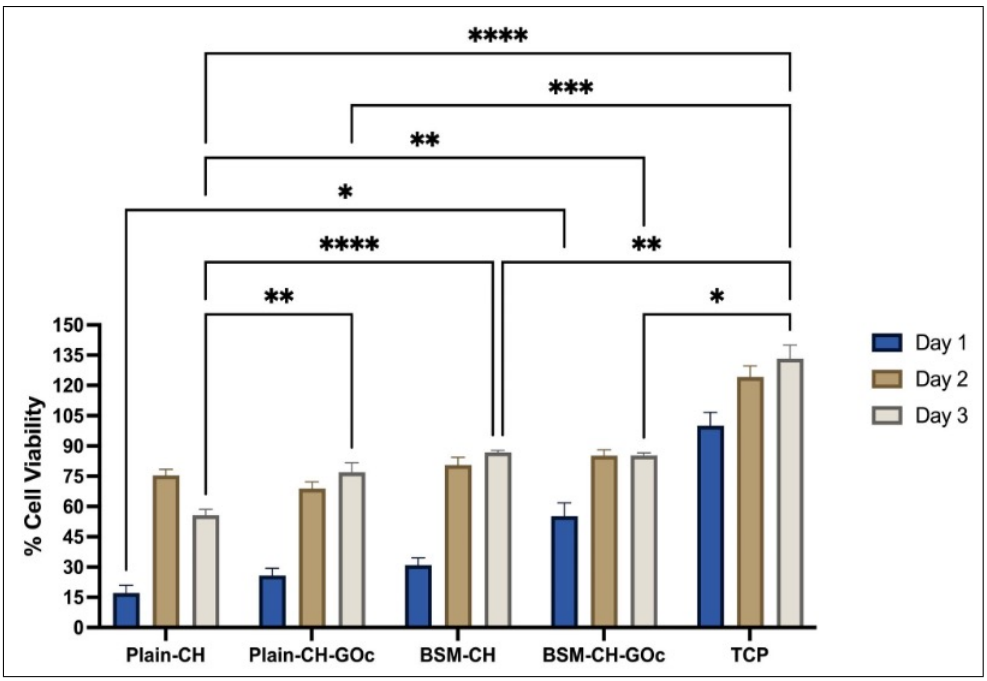

Figure 4.4 L929 cell viability (MTT assay) results of Plain-CH, Plain-CH-GOc, BSM-CH, BSM-CH-GOc membranes. (Mean ± SD, $^{*}p < 0.05, ^{**}p < 0.005, ^{***}p < 0.001, ^{****}p < 0.001, n = 3$.)

Statistical analysis indicates that loading ampicillin sodium salt on BSM-CH-GOc membranes increased cell viability significantly. Increasing Amp concentrations of membranes resulted in enhanced cell viability. Different concentrations of ampicillin sodium salt changed cell viability [$F(5, 10) = 18.23, p < 0.001$, two-way ANOVA; Figure 4.5A]. Effects of distinct concentrations of ampicillin were compared with multiple comparisons analysis. Fisher's LSD multiple comparisons were used to determine the difference between groups. It is indicated that the cell viability of the A1 and A3 membranes are significantly different from A0 on day1 [($p = 0.0108, p = 0.0179$), Fisher's LSD]. When it comes to differences on day 3, it is found that A3, A5 and A10 loaded membranes are significantly different from A0 for cell viability. [(Mean differences: 23.65, 26.35 and 43.06, respectively) ($p = 0.0005, p = 0.0299, p = 0.005$), Fisher's LSD].

Analysis of tetracycline hydrochloride-loaded groups demonstrated that the presence of tetra in the membranes reduced cell viability. In addition, increasing the concentration of tetra in membranes induce a significant decrease in cell viability [$F(5, 10) = 31.39, p < 0.001$, two-way ANOVA; Figure 4.5B]. Effects of distinct concentrations of tetracycline were compared with multiple comparisons analysis. Post hoc comparisons using the Dunnett's test indicated that the cell viability for the T0.5 [Mean difference = $39.95, p = 0.0349$], T1 [Mean difference = 45.99, $p = 0.0430$], T3 [Mean difference = $49.66, p = 0.0008$] was considerably less than the T0 on day 1. Besides, cell viability differences of Tetra loaded groups were considerably less than the T0 on day 3 for different concentrations, T0.5 [Mean difference = 54.57, $p = 0.0049$], T1 [Mean difference = 72.73, $p = 0.0006$], T3 [Mean difference = $78.85, p = 0.0010$] and T5 [Mean difference = 83.87, $p = 0.0001$].

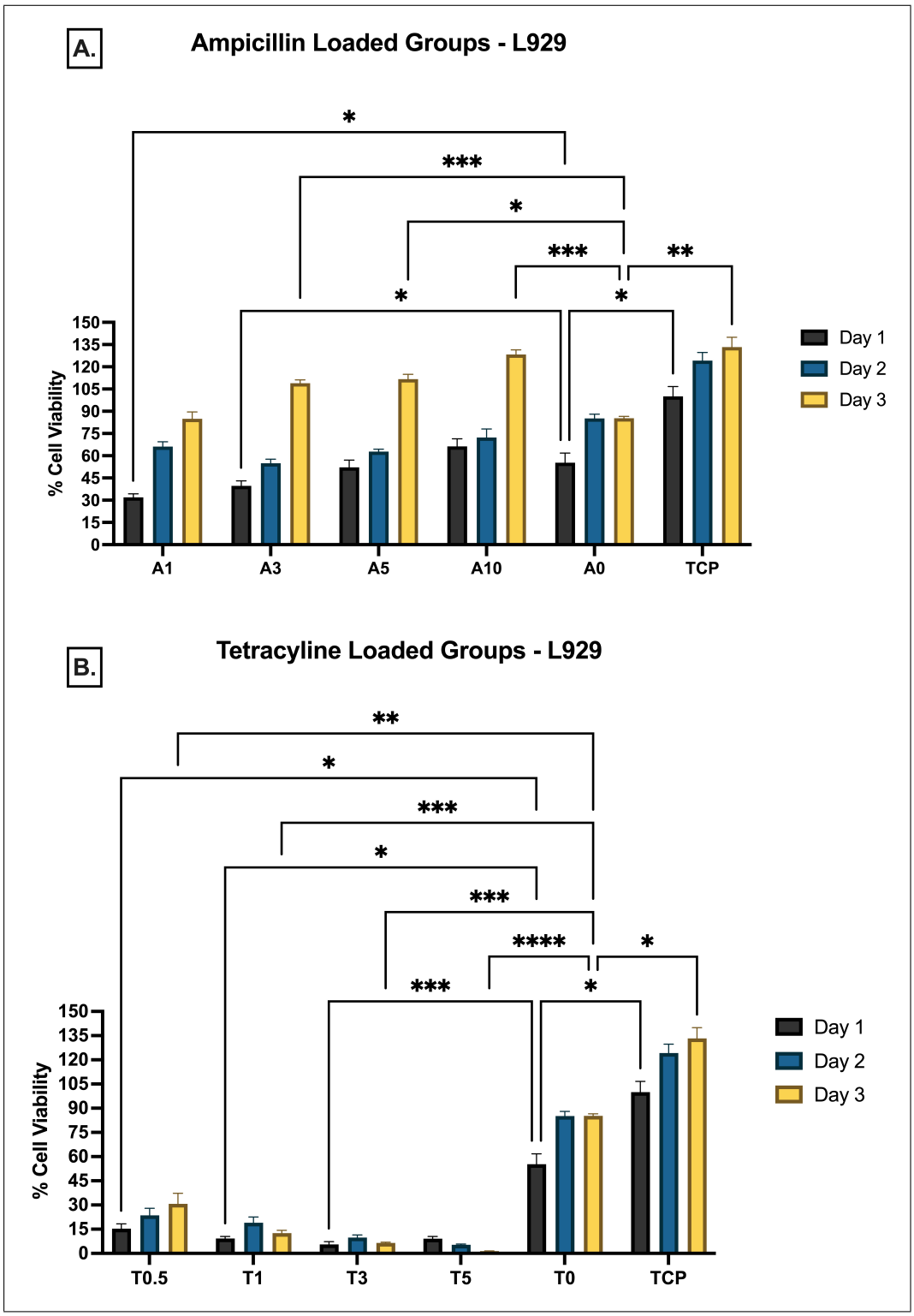

Figure 4.5 L929 cell viability results (A) MTT assay result of Ampicillin sodium salt loaded groups, (B) MTT assay of Tetracycline hydrochloride groups (A1: 1 $mgmL^{-1}$Amp, A3 : 3 $mgmL^{-1}$Amp, A5 : 5 $mgmLmp^{-1}$Amp, A10 : 10 mg mL^{-1} Amp loaded BSM-CH-GOc membranes, A0: Graphene Oxide coated bone surface mimicked chitosan membranes, Tetra: Tetracycline hydrochloride, T0.5: 0.5 $mgmL^{-1}$ Tetra, T1: 1 $mgmL^{-1}$Tetra, T3: 3 $mgmL^{-1}$Tetra, T5: 5 $mgmL^{-1}$Tetra membranes) (Mean $\pm$SD, $*p < 0.05, **p < 0.005, ***p < 0.001, ****p < 0.001, n = 3.$)

4.6 Bacteria Studies

4.6.1 *Staphylococcus Aureus* Biofilm Growth

Statistical analysis was used to quantify the *S.aureus* biofilm growth among groups. The Amp loaded groups' biofilm formation was shown to differ significantly from one another [$F(5, 10) = 5.789, p = 0.0112$, two-way ANOVA; Figure 4.6A]. The effects of various ampicillin concentrations were compared using Dunnett's multiple comparison analysis.

Increased concentration of Amp produced better results in reducing biofilm growth, with the highest reduction seen at A5 and A10 concentrations. On day 1, the biofilm growth rate of A1, A3, A5 and A10 was significantly lower than the control group (A0).The reductions in biofilm growth rate of *S.aureus* on Ampicillin loaded membranes on day 1 are as follows: A1(88%), A3(89%), A5(91%), A10(93%). Likewise, on day 3, the biofilm growth for A5 and A10 was significantly lower than the control group.

After quantifying the biofilm growth, statistical analysis shows that biofilm growth in tetracycline hydrochloride loaded membranes was significantly reduced compared to the control group [$F(5, 10) = 8.171, p = 0.0034$, two-way ANOVA; Figure 4.6B]. Furthermore, we observed that increasing the tetracycline concentration yields better results, with less biofilm growth (see T3 and T5 concentrations) at the end of the third quantification day. Different tetracycline concentrations' effects were compared using Dunnett's multiple comparisons approach. It was revealed that the *S. aureus*, biofilm growth for T0.5(94%), T1(95%), T3(96%) and T5(87%) was significantly lower than the T0 on day 1 . Accordingly, the biofilm formation was shown to be significantly lower for T0.5(50%), T1(54%), T3(69%), and T5(68%) on day 3 than the $T0$.

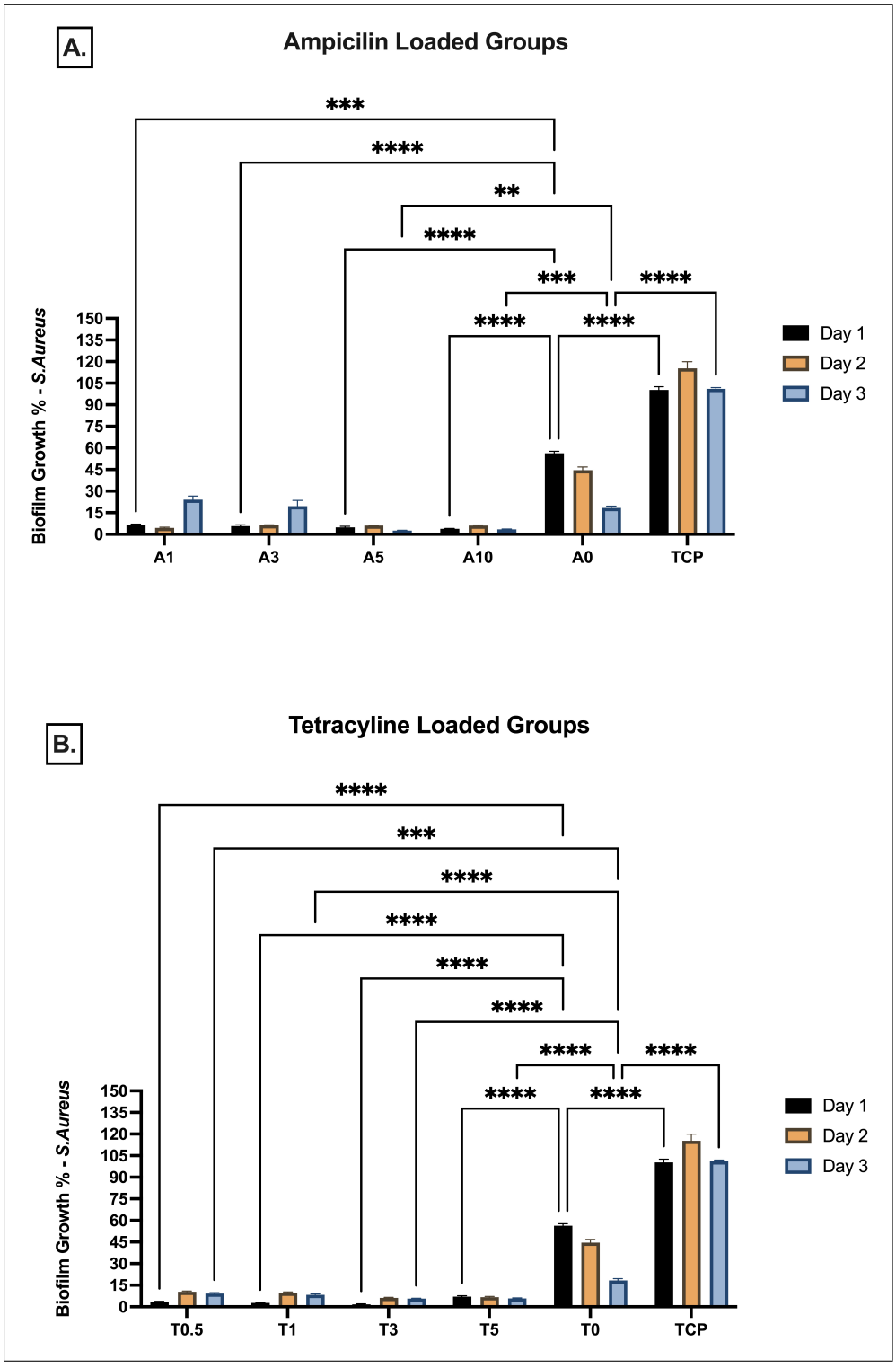

Figure 4.6 Bacterial biofilm growth of *S.aureus* in TBS (MTT assay). (A) MTT assay result of Ampicillin sodium salt loaded BSM-CH-GOc membranes, (B) MTT assay of Tetracycline hydrochloride loaded BSM-CH-GOc membranes (Mean $\pm$SD, $^{*}p < 0.05, ^{**}p < 0.005, ^{***}p < 0.001, ^{****}p < 0.001, n = 3$).

4.6.2 *Escherichia Coli* Biofilm Growth

The biofilm growth of the *E. coli* among Ampicillin loaded groups was measured using statistical analysis. We found that membrane loading with ampicillin sodium salt prevented the *E. coli* biofilm formation. Biofilm development in the groups that included different concentrations of ampicillin sodium salt and the control group differed significantly [$F(5, 10) = 9.584, p = 0.0019$, two way ANOVA; Figure 4.7A]. Additionally, it was found that higher ampicillin concentrations result in better outcomes and less biofilm development (see A3 and A10 concentrations). When all concentration levels of ampicillin were compared to the control group, a significant difference was found between the ampicillin groups at each level and the control group. Dunnett's test post hoc comparisons revealed that the biofilm formation of the A1(99%), A3(98%), A5(98%), and A10(95%) was substantially lower than the A0 on day 1. Similarly, biofilm growth of *E. coli* on Amp loaded membranes was significantly lower for the A1(38%), A3(56%), A5(50%), and A10(78%) on day 3 than for the A0.

Following quantification of biofilm growth of *E. coli*, statistical analysis reveals that biofilm growth in tetracycline hydrochloride loaded membranes was significantly lower than in the BSM-CH-GOc membranes (T0) [$F(5, 10) = 127.1, p = 0.00001$, two-way ANOVA Figure 4.7B]. Furthermore, it was observed that T1 and T3 tetracycline concentration results in better results with less biofilm growth at the end of the third quantification day. Biofilm growth differed significantly between the Tetracycline hydrochloride containing groups and the control group. Dunnett's test post hoc comparisons were conducted for various tetracycline concentration levels and the control group.On T0.5(98%), T1(97%), T3(94%), and T5(85%) significant biofilm growth decreases were observed when compared with T0 on day 1. Similar to day 1, in terms of *E.coli* biofilm growth on Tetra loaded groups on day 3, T0.5(87%), T1(89%), T3(88%), and T5(83%) had significantly lower growth compared to T0 (BSM-CH-GOc).

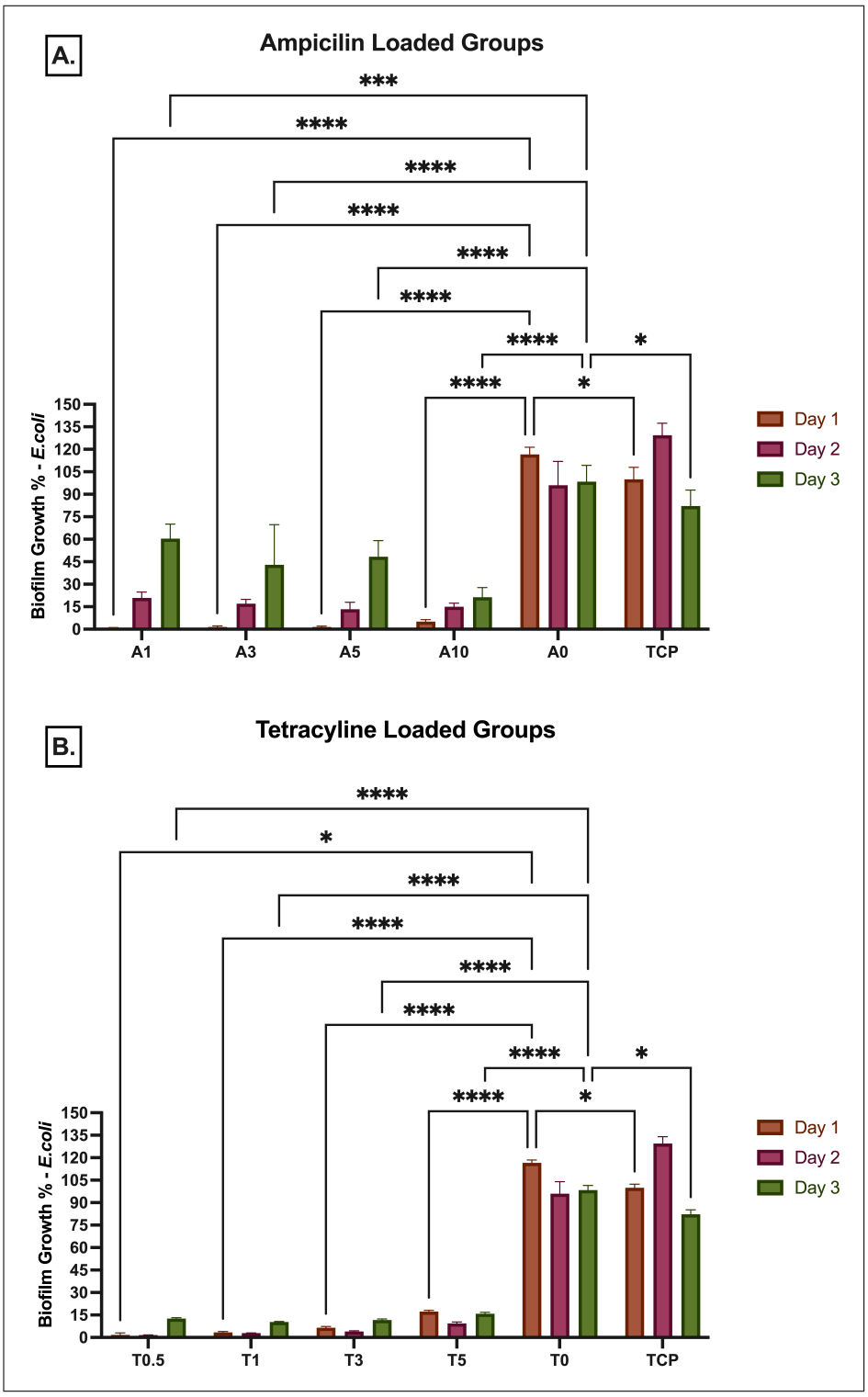

Figure 4.7 Bacterial biofilm growth of *E. coli* in LB (MTT assay). (A) MTT assay result of Ampicillin loaded BSM-CH-GOc membranes, (B) MTT assay of Tetracycline loaded BSM-CH-GOc membranes (Mean $\pm$SD, $^{*}p < 0.05, ^{**}p < 0.005, ^{***}p < 0.001, ^{****}p < 0.001, n = 3$).

4.7 Zone of Inhibition Test

The zone of inhibition was used to assess the bacterial inhibitory efficacy of Ampicillin sodium salt loaded BSM-CH-GOc and Tetracycline hydrochloride loaded BSM-CH-GOc membranes on the bacteria growth.

According to zone of inhibition results, it has been shown in Figure 4.9 that both *E. coli* and *S.aureus* are sensitive to antibiotics. It is also seen that the inhibition zone of the two antibiotics against both *S.aureus* and *E. coli* increases when the drug concentration increases in Figure 4.8 and Figure 4.9.

4.7.1 Zone of inhibition of the drug loaded membranes against *S.aureus*

To evaluate, one-way ANOVA was utilized, the ampicillin antibiotic concentration for measuring zones of inhibition [$F(3, 25) = 48.61, \mathrm{p} = 0.00001$ Figure 4.8A]. Except for A5-A3 dosage zones of inhibition analysis, all comparisons were statistically different. Determined zone diameter of Amp loaded BSM-CH-GOc membranes as follows: A1(33.42 ± 0.95), $A3(38.40 \pm 0.56)$, $A5(36.91 \pm 1.153)$, $A10(39.92 \pm 1.273)$.

Results of the measurement of zones of inhibition for the tetracycline antibiotic concentrations, [$\mathrm{F}(3, 25) = 37.87, \mathrm{p} = 0.00001$], are represented in Figure 4.8B. Statistical diameter of the bacteriostatic zone of Tetra loaded membranes T0.5, T1, T3, T5 against *S.aureus* are 20.47 ± 1.13, 22.75 ± 1.33, 25.76 ± 0.76, 26.30 ± 1.26 respectively. These findings imply that the ideal tetracycline dose is T5 in order to obtain the maximum zone inhibition measurement score.

4.7.2 Zone of inhibition of drug loaded membranes against *E.coli*

The antibiotic's location is surrounded by a zone of inhibition where bacterial colonies cannot flourish. In order to evaluate the ampicillin antibiotic concentration for

the measurement of zones of inhibition, one-way ANOVA was carried out [$F(3, 24) = 122.457, p = 0.00001$ Figure 4.8C]. All comparisons were significantly different except for A1-A3 dosage zones of inhibition measurement. Bacteria's susceptibility to different antibiotic concentration are 14.43 ± 0.64, 16.08 ± 0.42, 22.21 ± 1.27, 24.70 ± 0.87 for A1, A3, A5, and A10 in diameter respectively. These results indicate the best concentration for the best zone inhibition measurement score for A10.

Evaluation of zone of inhibition for tetracycline antibiotic concentration against *E.coli*, [$F(3, 23) = 52.16, p = 0.00001$] are represented in Figure 4.8D]. Except for T3-T1 dosage zones of inhibition assessment, all comparisons were statistically different. Statistical diameter of Tetracycline loaded BSM-CH-GOc membranes against *E.coli* as follows: $T0.5(18.29 \pm 0.91)$, $T1(20.15 \pm 0.51)$, $T3(20.81 \pm 0.79)$, $T5(23.11 \pm 0.45)$. These findings suggest that the optimal dose for tetracycline is T5 to achieve the highest zone inhibition measurement score.

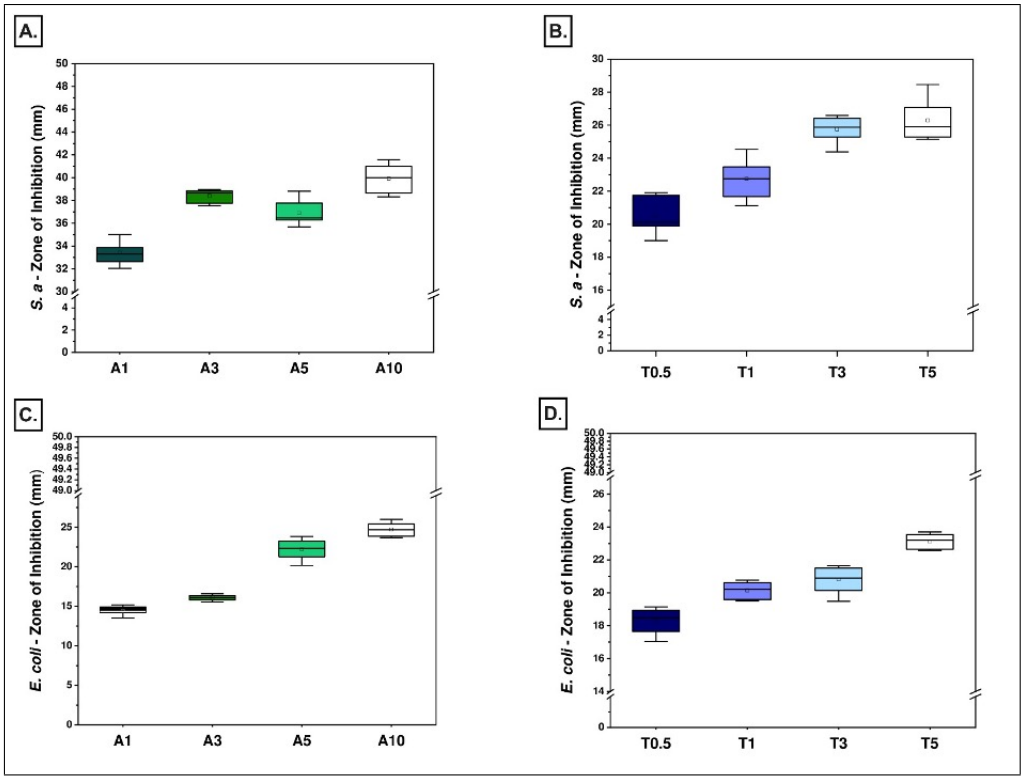

Figure 4.8 Statistical diameter of the bacteriostatic zones. (A) Zone of inhibition of Ampicillin loaded BSM-CH-GOc membranes against *S. aureus*, (B) Zone of inhibition of Tetracycline loaded BSM-CH-GOc membranes against *S. aureus*. (C) Zone of inhibition of Ampicillin loaded BSM-CH-GOc membranes against *E.coli*, (D) Zone of inhibition of Tetracycline loaded BSM-CH-GOc membranes against *E.coli*.

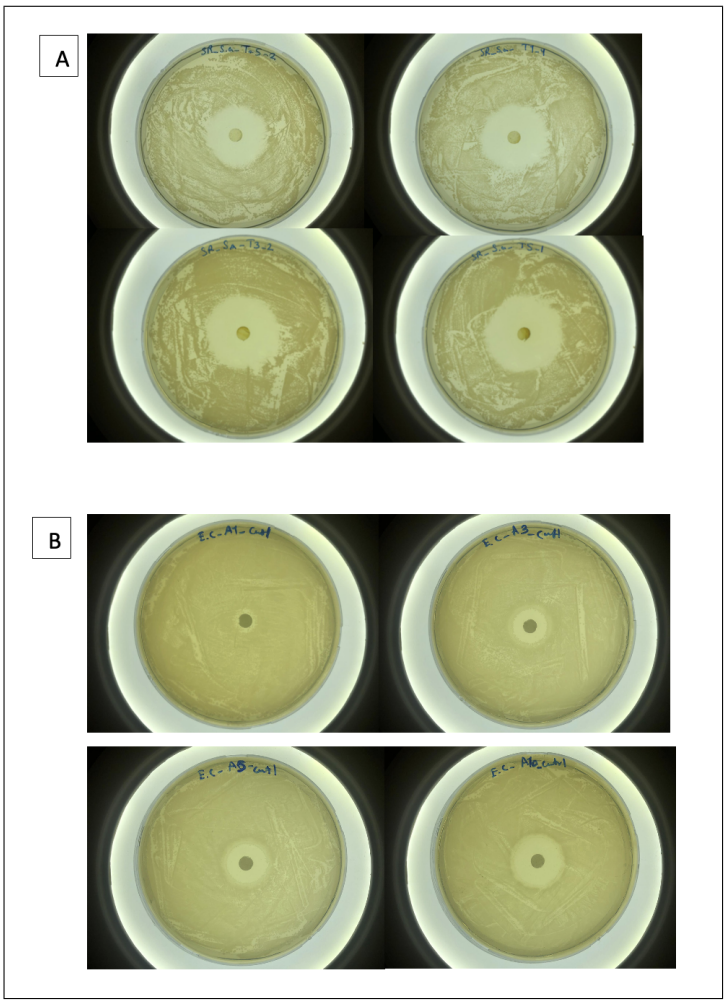

Figure 4.9 Zone of inhibition of drug loaded BSM-CH-GOc membranes on TSA plates (A) Zone of inhibition of Tetracycline hydrochloride loaded BSM-CH-GOc membranes against *S. aureus* on the plates. (B) Zone of inhibition of Ampicillin sodium salt loaded BSM-CH-GOc membranes against *E.coli* bacteria on the plates.

4.8 Statistical Analysis

Before conducting a hypothesis test, the normality and homogeneity of the thesis data were verified. Utilizing one-way, and two-way ANOVA, between-groups analyses for normally distributed data were carried out. Dunnett's, Tukey's and Fisher's LSD test post-hoc comparisons between the antibiotics and the control group were conducted after statistically significant main effects. The experiments were conducted in triplicate with n = 3 sample size.The result are reported as mean ± SD and $p < 0.05$ is used to establish statistical significance.

5. DISCUSSION

One of the most important stages in hampering prosthesis-related infection on biomaterial surfaces is to prevent the development and growth of bacterial biofilms. We studied cells with graphene oxide/CH and graphene oxide coating in the previous article, in which the power of GO coating to increase cell viability and proliferation is promising. Additionally, we observed that the formation of bacterial biofilms is likely prevented more effectively when GO is present as a surface coating on CH [46]. In an effort to create surfaces with better antibacterial capabilities and understand the impact of topography on bacteria behavior, graphene oxide coated membranes were selected for sample groups, and chitosan was chosen for bone surface mimicking. In order to evaluate these relationships between topography and surface-cell and surface-bacteria interactions and importance of each parameter, physicochemical characterization, cell culture and bacterial studies were conducted.

5.1 Material Characterization

Using the soft lithography technique, the topography of a bone was imitated (Figure 3.1). SEM images of femur bone, mold, and the BSM-CH membranes are depicted in Figure 4.1 and show that surface topography of bone was properly mimicked via soft lithography and solvent casting of chitosan.

Due to the fact that cells are in direct contact with surface characteristics, the wettability of a membrane surface is an important factor in biomaterial applications. The molecular interactions between materials and biological molecules in the surrounding tissue are influenced by the surface's wettability [48]. As shown in Table 4.1, Plain-CH membrane's water contact angle was determined to be $60.86\,^{\circ}$, which is consistent with published research [49]. The A10 membranes, with a water contact angle of $39.29\,^{\circ} \pm 2.75$, were regarded as the most hydrophilic. Tetra loaded mem-

branes are more hydrophobic, whereas membranes loaded with ampicillin are more hydrophilic. In addition, while GO in form of coating in Plain-CH membranes have impact on increasing the surface hydrophobicity, in the BM-CH membranes GO coating result in less hydrophilicity.

Chitosan's biodegradability is influenced by the level of deacetylation, the swelling properties, and the molecular weight [50]. Higher molecular weight chitosan is less soluble and degrades more slowly than lower molecular weight chitosan [51]. After three weeks of incubation in PBS, the weight loss of Amp and Tetra loaded BSM-CH-GOc membranes exhibits the maximum value. The PBS-incubated control samples demonstrated a comparable pattern of weight loss. Additionally, as shown in Figure 4.2C, surface coating with GO has a comparable impact on degradation. It is not unexpected that obtained lower weight loss (Tetra loaded and Amp loaded BSM- CH-GOc membranes degraded on average by 5.1% and 4.9%, respectively) because the chitosan-based membranes were tested with extremely high deacetylation degrees (92 - 97.5 %). This is because amine groups have a poor lysozyme susceptibility. Figure 4.2 shows the level of degradation of a chitosan-based membrane incubated in PBS.

One of the most crucial characteristics of the BSM-CH-GOc membranes was the drug release. The coupling of Amp with the almost any polymers has been the subject of several investigations, many of which have focused on developing effective pharmacokinetic drug delivery systems. The agar diffusion plate test was used to examine the antibacterial activity of fibers loaded with amp-loaded alginate and chitosan in one research. Results showed that the CH matrix allows the release of Amp into the environment and demonstrate its antimicrobial effect, in addition to Due to CH's capacity for crosslinking, which allowed for a larger uptake of Amp during the construction process, the antibacterial activity of the fiber was increased. Moreover, Y. Ciro et al. probed the antibacterial properties of Amp-Chitosan-Polyanion nanoparticles. They found that these nanoparticles were more effective at killing *S. aureus* bacteria than Ampicillin alone by using a broth micro-dilution method on both sensitive and resistant strains. This suggest that encapsulating Ampicillin in polymeric nanostructures can enhance drug release and improve its effectiveness [52]. Maximum cumulative

drug release observed in the first 24 hours. The maximum doses of ampicillin (A10) and tetracycline (T5) for drug release were significantly different from other doses, according to a detailed analysis of the Ampicillin and Tetracycline loaded membrane release profile. However, the doses of Amp and Tetra released from the BSM-CH-GOc membranes for the other doses (A1-A3-A5 and T0.5-T1-T3) did not differ statistically significantly (Figure 4.3). These results support the previous studies stated in the literature. Hao et al. used Tetracycline hydrochloride, a pharmacological model, was included into the citric modified chitosan hydrogel to improve its antibacterial capabilities. Tetra concentration was $3\,\mathrm{mgmL}^{-1}$. Increased antimicrobial effectiveness was seen against *E. coli* and *S. aureus* in the drug-loaded citric modified chitosan hydrogel. In experiments on animals, they found that the Tetra loaded hydrogel sped up the healing of wounds made on rats [53].

5.2 Cell Culture Studies

In elimination, cell viability test was performed using L929 cell line. After multiple comparisons of the four groups (Plain-CH, Plain-CH-GOc, BSM-CH and BSM-CH-GOc), the BSM-CH-GOc experimental group, the control group for the bacterial studies, was selected as the best (highest cell viability) as seen in Figure 4.4.

On chitosan-based membranes, L929 cell lines were grown, and the cell viability rate was measured to understand the cytotoxic effect of used two antibiotics. Three days were spent seeding cells. MTT tests were performed daily to measure the viability of the cells in the ampicillin and tetracycline groups in comparison to BSM-CH-GOc, the control. MTT is a technique that is frequently used to gauge the level of mitochondrial activity. The amount of viable cells is also thought to be reflected in the measurement [54]. TCP was used as a positive control for the experimental groups.

In terms of cell viability for Ampicillin groups compared to BSM-CH-GOc control group over three days, there is statistically remarkable difference between Ampicillin loaded membranes and the control group in the L929 cell line. Increasing Amp

concentrations of membranes resulted in enhanced cell viability. Regarding these findings, all ampicillin groups (A1, A3, A5, A10) showed L929 cell viability; this indicates that the proposed amounts of ampicillin groups have no cytotoxic effect on cell viability (Figure 4.5A).

In the L929 cell line, there is a statistically noticeable difference between the Tetracycline-loaded membranes and the BSM-CH-GOc control group in terms of cell viability over three days. While the T0.5 dosage of tetracycline led to the lowest cytotoxic effect on the L929 cells, T5 dosage of tetracycline had the highest cytotoxic effect on the L929 cells (Figure 4.5B). A significant difference between the groups was observed while comparing Plain-CH with BSM-CH and Plain-CH-GOc with the BSM-CH-GOc. In addition, comparison of BSM-CH and BSM-CH-GOc demonstrates a significant difference, which means that GO coating increased cell viability. These findings are supported by the the study of Kwak et al. [55]. The biological impact of graphene oxide on four different titanium surfaces were examined in their investigation. They demonstrated that the osteoblast differentiation, viability, and proliferation of bone marrow stromal cells are all markedly boosted by GO, and human gingival fibroblasts attachment and growth are also strengthened. Furthermore, osseointegration in vivo is significantly enhanced by GO coating of implant surfaces.

5.3 Bacteria Studies

Bacterial adhesion behavior is a very complicated process that is controlled by numerous mechanisms that depend on both the bacteria and the material. The bacteria specificity (gram negative or gram positive), and the composition of the cell wall, as well as the surface topography, porosity, wettability, surface chemistry all govern adhesion [56],[57]. The growth rate of the bacterial biofilm generated throughout a 72-hour incubation period was measured using the MTT test, which measures the metabolic activity of living bacteria. This test allowed for the quantitative measurement of biofilm formation for the *S. aureus* and *E. coli* strains, which are shown in Figure 4.6 and Figure 4.7. For the evaluation of *S. aureus* biofilm development after

3 days of cultivation, both Ampicillin sodium salt loaded membranes and Tetracycline hydrochloride loaded membranes have sinificantly lower biofilm formation than than BSM-CH-GOc membranes. It was found that the minimum biofilm growth of *S. aureus* on Amp-loaded membrane is A5 and A10, respectively (Figure 4.6A) and the minimum bacterial biofilm growth of *S. aureus* on Tetra-loaded membrane is T3 and T5, respectively (Figure 4.6B). Alavarse et al. shows that the tetracycline hydrochloride-loaded PVA and chitosan scaffolds could be applied as an antibacterial wound healing promoter. 5 mg/mL of tetracycline was used and effectiveness against bacteria of the scaffold on *Escherichia coli* and *Staphylococcus aureus* were tested in this study [58]. As a result of their differing cellular wall structures, the antibacterial activity is also more effective against the Gram-positive *S. aureus* than the Gram-negative *E. coli*. For electrospun nanofibrous PCL/PLA mats, Zahedi et al. similarly showed a similar rise in Tetracycline's antimicrobial effectiveness against *S. aureus* [59].

As for *E. coli* strain, on day 1, Ampicillin loaded groups were more effective the reducing bacterial growth than Tetra loaded groups, but results showed that Tetracycline loaded groups had statistically significantly less biofilm formation on day 3 compared to Amp loaded group. It was observed that A3 and A10, respectively, represent the lowest bacterial biofilm formation against *E. coli* on Amp-loaded membranes (Figure 4.7A). As shown in Figure 4.7B, the lowest *E. coli* bacterial biofilm formation on Tetra-loaded membrane was revealed to be T0.5 and T1, respectively. Based on study of Ozkahraman et al., a drug delivery system using chitosan polymers and NPs that were 0.5 mg/ml ampicillin antibiotic loaded demonstrated good antibacterial activity against *E. coli* [60].

Regarding biofilm MTT assay results, the groups with the same concentrations of Tetracycline were more potent against both *E. coli* and *S. aureus* than the groups loaded with Ampicillin. It is known from previous literature that the aromatic molecule is easily adsorbed on GO and graphene by $\pi - \pi$ stacking [61]. Tetracycline is made up of four aromatic rings, each of which has a different functional group. Tetracycline may be robustly deposited on the GO surface by cation- π bonding and contact. So, the intercalation of CH into GO might improve both the adsorption capability of

Tetra as well as the physical and chemical qualities derived synergistically from both components. These features may affect the antibacterial properties of Tetra containing membranes. Moreover, Tetracyclines attach to the 16S rRNA of the 30S subunit of the ribosome and they stop the formation of proteins by preventing aminoacyl tRNA from interacting with the A site on the mRNA-ribosome complex. Tetracyclines have a high degree of selectivity because they accumulate actively in bacterial cells but not in mammalian ones. Tetracyclines go within Gram-negative bacteria by passively diffusing through porin proteins in the outer membrane and then actively moving through the inner cytoplasmic membrane. Similar uptake into Gram-positive bacteria takes place via a transport system that depends on energy. Mammalian cells, in contrast, do not have the active transport system found in sensitive bacteria [62]. These mechanisms of tetracycline explain why it gave different results against *E. coli* and *S. aureus* in this thesis.

To verify the result of the biofilm experiment, the zone of inhibition experiment was conducted. These findings support Figure 4.9's and Figures 4.8's assertion that when drug concentration rises, the inhibition zones of the two antibiotics against *S. aureus* and *E. coli* expand. This result shows that bacteria are sensitive to antibiotics and is supported by literature [53], [63].

5.4 Conclusion

Orthopedic implants have greatly aided in the functional recovery of patients with bone fractures or other anomalies; nevertheless, if an infection occurs, the implant will fail, and another surgery will be needed. Evidence indicates that prosthesis infections are biofilm-correlated infections. Additionally, if initial bacterial attachment and development on the surface can be prevented, bacterial biofilm formation can be restrained.

In this thesis, surface microstructure of bone surface was mimicked onto CH membranes with remarkable precision. Degradation rates were shown to be influ-

enced by drug loading and surface coating. In elimination, the cell viability test was performed using a mouse fibroblast (L929) cell line. Accordingly, BSM-CH-GOc experimental group was selected as the best group after three days which was the control group for the bacterial studies. Additionally, bacterial biofilm test result showed an effective reduction in bacterial biofilm formation in both bacterial strains using Amp and Tetra antibiotics. The zone of inhibition on solid agar plates supported the biofilm result giving a similar trend. In light of these findings, it is concluded that methods for optimizing cell implant interactions and minimizing bacteria-implant interaction by chemical changes of material surfaces and physical surface topography can be improved.

REFERENCES

1. James Browne, MD, F., "American joint replacement registry 2021 annual report.," *American Academy of Orthopaedic Surgeons (AAOS)*, pp. 55, 90, 91, 2021.

2. Metsemakers, W., R. Kuehl, T. Moriarty, R. Richards, M. Verhofstad, O. Borens, S. Kates, and M. Morgenstern, "Infection after fracture fixation: current surgical and microbiological concepts," *Injury*, Vol. 49, no. 3, pp. 511–522, 2018.

3. Stewart, P. S., "Antimicrobial tolerance in biofilms," *Microbiology Spectrum*, Vol. 3, no. 3, pp. 3–5, 2015.

4. Liang, J., H. Wang, and M. Libera, "Biomaterial surfaces self-defensive against bacteria by contact transfer of antimicrobials," *Biomaterials*, Vol. 204, pp. 25–35, 2019.

5. Wang, Y., Y. Zhou, X. Wang, Y. Liu, S. Wen, X. Zheng, and P. Wang, "Cytocompatibility and in vivo biodegradation of graphene-modified chitosan 3d porous scaffold," *Materials Letters*, Vol. 220, pp. 1–4, 2018.

6. Ahmed, J., M. Mulla, and M. Maniruzzaman, "Rheological and dielectric behavior of 3d-printable chitosan/graphene oxide hydrogels," *ACS Biomaterials Science & Engineering*, Vol. 6, no. 1, pp. 88–99, 2019.

7. Parhi, R., "Drug delivery applications of chitin and chitosan: a review," *Environmental Chemistry Letters*, Vol. 18, no. 3, pp. 577–594, 2020.

8. Rezaei, F. S., F. Sharifianjazi, A. Esmaeilkhanian, and E. Salehi, "Chitosan films and scaffolds for regenerative medicine applications: A review," *Carbohydrate Polymers*, Vol. 273, 2021.

9. Liu, H., C. Wang, C. Li, Y. Qin, Z. Wang, F. Yang, Z. Li, and J. Wang, "A functional chitosan-based hydrogel as a wound dressing and drug delivery system in the treatment of wound healing," *RSC Advances*, Vol. 8, no. 14, pp. 7533–7549, 2018.

10. El Knidri, H., R. Belaabed, A. Addaou, A. Laajeb, and A. Lahsini, "Extraction, chemical modification and characterization of chitin and chitosan," *International Journal of Biological Macromolecules*, Vol. 120, pp. 1181–1189, 2018.

11. Mohammed, M. A., J. T. Syeda, K. M. Wasan, and E. K. Wasan, "An overview of chitosan nanoparticles and its application in non-parenteral drug delivery," *Pharmaceutics*, Vol. 9, no. 4, p. 53, 2017.

12. Tekade, R. K., R. Maheshwari, and M. Tekade, "Biopolymer-based nanocomposites for transdermal drug delivery," in *Biopolymer-Based Composites*, pp. 81–106, Elsevier, 2017.

13. Yang, X., Y. Tu, L. Li, S. Shang, and X.-m. Tao, "Well-dispersed chitosan/graphene oxide nanocomposites," *ACS Applied Materials & Interfaces*, Vol. 2, no. 6, pp. 1707–1713, 2010.

14. Kesavan, S., K. Meena, S. A. Sharmili, M. Govindarajan, N. S. Alharbi, S. Kadaikunnan, J. M. Khaled, A. S. Alobaidi, K. F. Alanzi, and B. Vaseeharan, "Ulvan loaded graphene oxide nanoparticle fabricated with chitosan and d-mannose for targeted anticancer drug delivery," *Journal of Drug Delivery Science and Technology*, Vol. 65, 2021.

15. Eivazzadeh-Keihan, R., A. Maleki, M. De La Guardia, M. S. Bani, K. K. Chenab, P. Pashazadeh-Panahi, B. Baradaran, A. Mokhtarzadeh, and M. R. Hamblin, "Carbon based nanomaterials for tissue engineering of bone: Building new bone on small black scaffolds: A review," *Journal of Advanced Research*, Vol. 18, pp. 185–201, 2019.

16. Ali, I. H., A. Ouf, F. Elshishiny, M. B. Taskin, J. Song, M. Dong, M. Chen, R. Siam, and W. Mamdouh, "Antimicrobial and wound-healing activities of graphene-reinforced electrospun chitosan/gelatin nanofibrous nanocomposite scaffolds," *ACS Omega*, Vol. 7, no. 2, pp. 1838–1850, 2022.

17. Hosseini, S. M., M. Abdouss, S. Mazinani, A. Soltanabadi, and M. Kalaee, "Modified nanofiber containing chitosan and graphene oxide-magnetite nanoparticles as effective materials for smart wound dressing," *Composites Part B: Engineering*, Vol. 231, 2022.

18. Xue, J., C. Feng, L. Xia, D. Zhai, B. Ma, X. Wang, B. Fang, J. Chang, and C. Wu, "Assembly preparation of multilayered biomaterials with high mechanical strength and bone-forming bioactivity," *Chemistry of Materials*, Vol. 30, no. 14, 2018.

19. "National center for biotechnology information," *"PubChem Compound Summary for CID 23663979, Ampicillin sodium" PubChem, https://pubchem.ncbi.nlm.nih.gov/compound/Ampicillin-sodium.*, 2022.

20. Ahn, S., C. Mun, and S. Lee, "Microfluidic spinning of fibrous alginate carrier having highly enhanced drug loading capability and delayed release profile," *RSC Advances*, Vol. 5, no. 20, 2015.

21. "National center for biotechnology information," *"PubChem Compound Summary for CID 54704426, Tetracycline hydrochloride" PubChem, https://pubchem.ncbi.nlm.nih.gov/compound/Tetracycline-HCl.*, 2022.

22. El-Alfy, E. A., M. K. El-Bisi, G. M. Taha, and H. M. Ibrahim, "Preparation of biocompatible chitosan nanoparticles loaded by tetracycline, gentamycin and ciprofloxacin as novel drug delivery system for improvement the antibacterial properties of cellulose based fabrics," *International Journal of Biological Macromolecules*, Vol. 161, pp. 1247–1260, 2020.

23. Hall-Stoodley, L., J. W. Costerton, and P. Stoodley, "Bacterial biofilms: from the natural environment to infectious diseases," *Nature Reviews Microbiology*, Vol. 2, no. 2, pp. 95–108, 2004.

24. Muhammad, M. H., A. L. Idris, X. Fan, Y. Guo, Y. Yu, X. Jin, J. Qiu, X. Guan, and T. Huang, "Beyond risk: bacterial biofilms and their regulating approaches," *Frontiers in Microbiology*, Vol. 11, p. 928, 2020.

25. Stewart, P. S., "Antimicrobial tolerance in biofilms," *Microbiology Spectrum*, Vol. 3, no. 3, pp. 3–3, 2015.

26. Dörr, T., P. J. Moynihan, and C. Mayer, "Bacterial cell wall structure and dynamics," 2019.

27. Miller, K. P., L. Wang, B. C. Benicewicz, and A. W. Decho, "Inorganic nanoparticles engineered to attack bacteria," *Chemical Society Reviews*, Vol. 44, no. 21, pp. 7787–7807, 2015.

28. Baek, Y.-W., and Y.-J. An, "Microbial toxicity of metal oxide nanoparticles (cuo, nio, zno, and sb2o3) to escherichia coli, bacillus subtilis, and streptococcus aureus," *Science of the Total Environment*, Vol. 409, no. 8, pp. 1603–1608, 2011.

29. Romaniuk, J. A., and L. Cegelski, "Bacterial cell wall composition and the influence of antibiotics by cell-wall and whole-cell nmr," *Philosophical Transactions of the Royal Society B: Biological Sciences*, Vol. 370, no. 1679, 2015.

30. Cobos, M., B. González, M. J. Fernández, and M. D. Fernández, "Chitosan–graphene oxide nanocomposites: Effect of graphene oxide nanosheets and glycerol plasticizer on thermal and mechanical properties," *Journal of Applied Polymer Science*, Vol. 134, no. 30, 2017.

31. Zhang, S., B. Ma, S. Wang, J. Duan, J. Qiu, D. Li, Y. Sang, S. Ge, and H. Liu, "Mass-production of fluorescent chitosan/graphene oxide hybrid microspheres for in vitro 3d expansion of human umbilical cord mesenchymal stem cells," *Chemical Engineering Journal*, Vol. 331, pp. 675–684, 2018.

32. Valencia, C., C. H. Valencia, F. Zuluaga, M. E. Valencia, J. H. Mina, and C. D. Grande-Tovar, "Synthesis and application of scaffolds of chitosan-graphene oxide by the freeze-drying method for tissue regeneration," *Molecules*, Vol. 23, no. 10, p. 2651, 2018.

33. Zhang, L., X. Li, C. Shi, G. Ran, Y. Peng, S. Zeng, and Y. He, "Biocompatibility and angiogenic effect of chitosan/graphene oxide hydrogel scaffolds on epcs," *Stem Cells International*, Vol. 2021, 2021.

34. Khalil, W. F., G. S. El-Sayyad, W. M. El Rouby, M. Sadek, A. A. Farghali, and A. I. El-Batal, "Graphene oxide-based nanocomposites (go-chitosan and go-edta) for outstanding antimicrobial potential against some candida species and pathogenic bacteria," *International Journal of Biological Macromolecules*, Vol. 164, pp. 1370–1383, 2020.

35. Solìs Moré, Y., G. Panella, G. Fioravanti, F. Perrozzi, M. Passacantando, F. Giansanti, M. Ardini, L. Ottaviano, A. Cimini, C. Peniche, *et al.*, "Biocompatibility of composites based on chitosan, apatite, and graphene oxide for tissue applications," *Journal of Biomedical Materials Research Part A*, Vol. 106, no. 6, pp. 1585–1594, 2018.

36. Valencia, A. M., C. H. Valencia, F. Zuluaga, and C. D. Grande-Tovar, "Synthesis and fabrication of films including graphene oxide functionalized with chitosan for regenerative medicine applications," *Heliyon*, Vol. 7, no. 5, 2021.

37. Liu, X., Y. Wu, X. Zhao, and Z. Wang, "Fabrication and applications of bioactive chitosan-based organic-inorganic hybrid materials: A review," *Carbohydrate Polymers*, Vol. 267, 2021.

38. Francolini, I., E. Perugini, I. Silvestro, M. Lopreiato, A. Scotto dâAbusco, F. Valentini, E. Placidi, F. Arciprete, A. Martinelli, and A. Piozzi, "Graphene oxide oxygen content affects physical and biological properties of scaffolds based on chitosan/graphene oxide conjugates," *Materials*, Vol. 12, no. 7, p. 1142, 2019.

39. Wang, C., Z. Zhang, B. Chen, L. Gu, Y. Li, and S. Yu, "Design and evaluation of galactosylated chitosan/graphene oxide nanoparticles as a drug delivery system," *Journal of Colloid and Interface Science*, Vol. 516, pp. 332–341, 2018.

40. Qiao, F., J. Ke, Y. Liu, B. Pei, Q. Hu, B. Z. Tang, and Z. Wang, "Cationic quaternized chitosan bioconjugates with aggregation-induced emission features for cell imaging," *Carbohydrate Polymers*, Vol. 230, 2020.

41. Puza, F., S. Rostami, B. Özçolak-Aslan, S. Odabaş, K. D. Jandt, and B. Garipcan, "Anisotropic bone surface topography mimicked chitosan/graphene oxide membranes," *Advanced Engineering Materials*, 2022.

42. Valencia Zapata, M. E., J. H. Mina Hernandez, C. D. Grande Tovar, C. H. Valencia Llano, J. A. Diaz Escobar, B. Vázquez-Lasa, J. San Román, and L. Rojo, "Novel bioactive and antibacterial acrylic bone cement nanocomposites modified with graphene oxide and chitosan," *International Journal of Molecular Sciences*, Vol. 20, no. 12, p. 2938, 2019.

43. Pandele, A. M., S. Dinescu, M. Costache, E. Vasile, C. Obreja, H. Iovu, and M. Ionita, "Preparation and in vitro, bulk, and surface investigation of chitosan/graphene oxide composite films," *Polymer Composites*, Vol. 34, no. 12, pp. 2116–2124, 2013.

44. Su, J., Z. Du, L. Xiao, F. Wei, Y. Yang, M. Li, Y. Qiu, J. Liu, J. Chen, and Y. Xiao, "Graphene oxide coated titanium surfaces with osteoimmunomodulatory role to enhance osteogenesis," *Materials Science and Engineering*, Vol. 113, 2020.

45. Liu, H., K. K. Leonas, and Y. Zhao, "Antimicrobial properties and release profile of ampicillin from electrospun poly (εepsilon;-caprolactone) nanofiber yarns," *Journal of Engineered Fibers and Fabrics*, Vol. 5, no. 4, 2010.

46. Rostami, S., F. Puza, M. Ucak, E. Ozgur, O. Gul, U. K. Ercan, and B. Garipcan, "Bifunctional sharkskin mimicked chitosan/graphene oxide membranes: Reduced biofilm formation and improved cytocompatibility," *Applied Surface Science*, Vol. 544, 2021.

47. Masri, A., D. M. Brown, D. G. Smith, V. Stone, and H. J. Johnston, "Comparison of in vitro approaches to assess the antibacterial effects of nanomaterials," *Journal of Functional Biomaterials*, Vol. 13, no. 4, p. 255, 2022.

48. Chan, C.-W., L. Carson, G. C. Smith, A. Morelli, and S. Lee, "Enhancing the antibacterial performance of orthopaedic implant materials by fibre laser surface engineering," *Applied Surface Science*, Vol. 404, pp. 67–81, 2017.

49. Alghuwainem, Y. A., M. Gouda, M. M. Khalaf, A. Elmushyakhi, M. F. Abou Taleb, and H. M. A. El-Lateef, "Synthesis and characterization of chitosan-containing zns/zro2/graphene oxide nanocomposites and their application in wound dressing," *Polymers*, Vol. 14, no. 23, p. 5195, 2022.

50. Lončarević, A., M. Ivanković, and A. Rogina, "Lysozyme-induced degradation of chitosan: the characterisation of degraded chitosan scaffolds," *J. Tissue Repair Regen*, Vol. 1, pp. 12–22, 2017.

51. Garg, U., S. Chauhan, U. Nagaich, and N. Jain, "Current advances in chitosan nanoparticles based drug delivery and targeting," *Advanced Pharmaceutical Bulletin*, Vol. 9, no. 2, p. 195, 2019.

52. Ciro, Y., J. Rojas, J. Oñate-Garzon, and C. H. Salamanca, "Synthesis, characterisation and biological evaluation of ampicillin–chitosan–polyanion nanoparticles produced by ionic gelation and polyelectrolyte complexation assisted by high-intensity sonication," *Polymers*, Vol. 11, no. 11, p. 1758, 2019.

53. Chen, H., B. Li, B. Feng, H. Wang, H. Yuan, and Z. Xu, "Tetracycline hydrochloride loaded citric acid functionalized chitosan hydrogel for wound healing," *RSC Advances*, Vol. 9, no. 34, pp. 19523–19530, 2019.

54. Rai, Y., R. Pathak, N. Kumari, D. K. Sah, S. Pandey, N. Kalra, R. Soni, B. Dwarakanath, and A. N. Bhatt, "Mitochondrial biogenesis and metabolic hyperactivation limits the application of mtt assay in the estimation of radiation induced growth inhibition," *Scientific Reports*, Vol. 8, no. 1, pp. 1–15, 2018.

55. Kwak, J. M., J. Kim, C.-S. Lee, I.-S. Park, M. Lee, D.-H. Min, and I.-S. L. Yeo, "Graphene oxide as a biocompatible and osteoinductive agent to promote implant osseointegration in a rabbit tibia model," *Advanced Materials Interfaces*, Vol. 9, no. 28, 2022.

56. Bohinc, K., G. Dražić, M. Oder, M. Jevšnik, D. Nipič, K. Godič-Torkar, P. Raspor, *et al.*, "Available surface dictates microbial adhesion capacity," *International Journal of Adhesion and Adhesives*, Vol. 50, pp. 265–272, 2014.

57. Tripathy, A., P. Sen, B. Su, and W. H. Briscoe, "Natural and bioinspired nanostructured bactericidal surfaces," *Advances in Colloid and Interface Science*, Vol. 248, pp. 85–104, 2017.

58. Alavarse, A. C., F. W. de Oliveira Silva, J. T. Colque, V. M. da Silva, T. Prieto, E. C. Venancio, and J.-J. Bonvent, "Tetracycline hydrochloride-loaded electrospun nanofibers mats based on pva and chitosan for wound dressing," *Materials Science and Engineering: C*, Vol. 77, pp. 271–281, 2017.

59. Zahedi, P., Z. Karami, I. Rezaeian, S.-H. Jafari, P. Mahdaviani, A. H. Abdolghaffari, and M. Abdollahi, "Preparation and performance evaluation of tetracycline hydrochloride loaded wound dressing mats based on electrospun nanofibrous poly (lactic acid)/poly caprolactone blends," *Journal of Applied Polymer Science*, Vol. 124, no. 5, pp. 4174–4183, 2012.

60. Özkahraman, B., E. Tamahkar, N. İdil, A. Kılıç Suloglu, and I. Perçin, "Evaluation of hyaluronic acid nanoparticle embedded chitosan–gelatin hydrogels for antibiotic release," *Drug Development Research*, Vol. 82, no. 2, pp. 241–250, 2021.

61. Lin, Y., S. Xu, and J. Li, "Fast and highly efficient tetracyclines removal from environmental waters by graphene oxide functionalized magnetic particles," *Chemical Engineering Journal*, Vol. 225, pp. 679–685, 2013.

62. Golan, D. E., A. H. Tashjian, and E. J. Armstrong, *Principles of Pharmacology: The Pathophysiologic Basis of Drug Therapy*, Lippincott Williams & Wilkins, 2011.

63. Salamanca, C. H., Á. Barrera-Ocampo, and J. Oñate-Garzón, "Development, characterization, and antimicrobial evaluation of ampicillin-loaded nanoparticles based on poly (maleic acid-co-vinylpyrrolidone) on resistant staphylococcus aureus strains," *Molecules*, Vol. 27, no. 9, p. 2943, 2022.